ACS APPLIED MATERIALS & INTERFACES

Research Article

www.acsami.org

Solvent-Assisted Oxygen Incorporation of Vertically Aligned MoS_2 Ultrathin Nanosheets Decorated on Reduced Graphene Oxide for Improved Electrocatalytic Hydrogen Evolution

Aiping Liu,*[,†,‡] Li Zhao,[†] Junma Zhang,[†] Liangxu Lin,[§] and Huaping Wu[∥]

[†]Center for Optoelectronics Materials and Devices, Zhejiang Sci-Tech University, Hangzhou 310018, China

[‡]State Key Laboratory of Nonlinear Mechanics, Institute of Mechanics, Chinese Academy of Sciences, Beijing 100190, China

[§]College of Engineering, Mathematics and Physical Sciences, University of Exeter, Exeter, EX4 4QL, U.K.

[∥]A Key Laboratory of E&M (Zhejiang University of Technology), Ministry of Education & Zhejiang Province, Hangzhou 310014, China

Supporting Information

ABSTRACT: Three-dimensional oxygen-incorporated MoS_2 ultrathin nanosheets decorated on reduced graphene oxide (O-MoS_2/rGO) had been successfully fabricated through a facile solvent-assisted hydrothermal method. The origin of the incorporated oxygen and its incorporation mechanism into MoS_2 were carefully investigated. We found that the solvent *N*,*N*-dimethylformamide (DMF) was the key as the reducing agent and the oxygen donor, expanding interlayer spaces and improving intrinsic conductivity of MoS_2 sheets (modulating its electronic structure and vertical edge sites). These O dopants, vertically aligned edges and decoration with rGO gave effectively improved double-layer capacitance and catalytic performance for hydrogen evolution reaction (HER) of MoS_2. The prepared O-MoS_2/rGO catalysts showed an exceptional small Tafel slope of 40 mV/decade, a high current density of 20 mA/cm^2 at the overpotential of 200 mV and remarkable stability even after 2000th continuous HER test in the acid media.

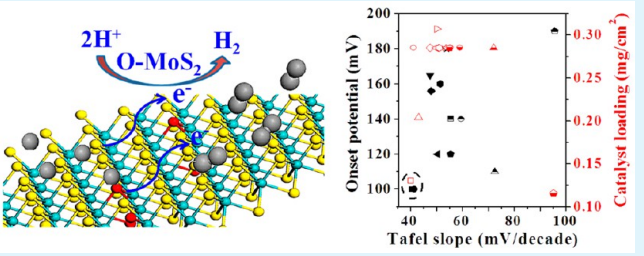

KEYWORDS: *oxygen incorporation, vertically aligned, MoS_2 nanosheets, graphene oxide, hydrogen evolution, electrochemistry*

1. INTRODUCTION

Electrochemical hydrogen evolution reaction (HER) is considered as one of the most promising techniques to combating global challenges of climate change and energy crisis.[1−5] Up to now, platinum (Pt) group metals are considered as the most efficient electrochemical catalysts for HER due to the exceptionally low overpotential near the thermodynamic potential of HER.[6−16] However, the high cost and low abundance prohibit their potential utilization.

Tremendous efforts on developing alternative cost-effective HER catalysts are not very successful, but recent progresses on molybdenum disulfide (MoS_2) are more encouraging.[16−25] Theoretically, MoS_2 has comparable catalytic activity to Pt and has been regarded as an ideal catalyst for HER.[26] The catalytic activity of MoS_2 highly depends on its catalytically active exposed edges.[3,10] Many works have been conducted to improve the edge ratio of MoS_2, including the formation of nanostructured and monolayered MoS_2 sheets by different techniques (e.g., chemical vapor deposition,[27−29] hydrothermal,[1,30−32] wet chemical,[33] thermal decomposition,[22] electrochemical deposition,[8,34] and ball milling methods).[11] However, the extremely low electrical conductivity of MoS_2 nanostructure, especially along the adjacent interlayers, which is about 2 orders of magnitude lower than that of vertically stacked S−Mo−S planes,[2,13] hampers the electron transfer for highly efficient HER. Further improvement of the HER performance of MoS_2 is challenging, but it is possible by modulating the electronic structure via element doping[35−40] and introducing highly conductive material (e.g., graphene, carbon nanotubes, carbon cloth, and amorphous carbon) to build hybrid structures and facilitate electron transfer process at the interfaces.[1,18,19,41] Recently, modulating the layer and electronic structures of MoS_2 through doping at both atomic and molecular levels has triggered intensive research interests. For example, Merki et al. proposed a cation intercalating strategy and obtained metal ions incorporated amorphous MoS_2 films, which optimized the catalytic activity by additional S edge sites.[25] Bao and his co-workers enhanced the H adsorption ability of in-plane S atoms by a single-atom metal doping into MoS_2 nanosheets.[36] The strategies by introducing anions into the adjacent layers of MoS_2 or substituting the S atoms also lead to the improved intrinsic conductivity and

Received: May 22, 2016
Accepted: September 7, 2016
Published: September 7, 2016

DOI: 10.1021/acsami.6b06031
ACS Appl. Mater. Interfaces 2016, 8, 25210−25218

accelerated proton adsorption. Thereinto, oxygen incorporation is considered as an effective route to facilitating the HER performance by engineering the surface disorder of MoS_2 with additional active sites.[4,6,14,40] However, the exact origin of the incorporated oxygen from chemical precursors[6,40] or oxygen-containing groups (e.g., graphene oxide/GO)[14] and the associated incorporation process are still controversial and inconclusive.

Herein, we demonstrated a one-step, solvent-assisted hydrothermal technique to easy fabricate three-dimensional (3D), vertically aligned and oxygen-incorporated MoS_2 nanosheets anchored on reduced GO (O-MoS_2/rGO). We showed how this preparation, O-incorporation and introduction of rGO effectively improved the HER performance of MoS_2 catalysts. As shown in Scheme 1, freeze-dried GO power and

Scheme 1. Diagram Shows the Growth of Vertically Aligned O-MoS_2/rGO Catalysts

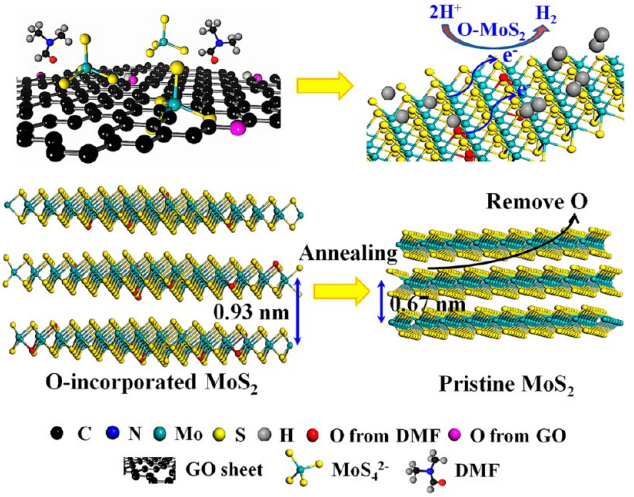

$(NH_4)_2MoS_4$ precursor was dispersed in the solvent *N*,*N*-dimethylformamide (DMF). The $(NH_4)_2MoS_4$ precursor was first anchored on GO sheet driven by the formation of C═S/C−S, giving crystal seeds for MoS_2 nucleation.[21] Mo(VI) was reduced to Mo(IV) by DMF (GO was also reduced to rGO to certain extent) to form MoS_2 nanosheets which further assembled into 3D nanoflowers to minimize the total surface energy. Besides, DMF also served as oxygen donor, introducing the O element into MoS_2 structure with enlarged interlayer space (~0.93 nm) which restored to 0.67 nm upon annealing at 500 °C due to the removal of the O dopant. Additionally, DMF was found to adjust and engineer disorder degree of O-MoS_2 by simply changing the amount of DMF in the reaction system. With the increased exposed vertical edge ratio, effective active surface area (EASA) and improved electron transport of MoS_2, remarkable stable HER performance (negligible loss even after continuous 2000 cycles) with a high current density of 20 mA/cm^2 (at 200 mV versus reversible hydrogen electrode, RHE) and small Tafel slope (40 mV/decade) were achieved.

2. EXPERIMENTAL SECTION

2.1. Preparation and Structure Modulation of Vertically Aligned O-MoS_2/rGO Catalysts in the DMF Solvent. GO was prepared by a modified Hummers' method[42] and dried in a freeze-dryer for 48 h. The O-MoS_2/rGO catalysts were synthesized through the one-step solvent-assisted hydrothermal method. Briefly, 10 mg of the as-prepared freeze-dried GO power was dispersed in 10 mL DMF. The mixture was then sonicated at room temperature for approximately 15 min to obtain a clear and homogeneous solution. After that, 20 mg of $(NH_4)_2MoS_4$ was added to the suspension, followed by sonicating for another 15 min until the scarlet solution was achieved. The reaction solution was then transferred to a 25 mL Teflon-lined autoclave and kept in an oven at 190 °C for 15 h. The obtained black product was collected by centrifugation at 8000 rpm for 8 min with ethanol and deionized water for several times to remove any impurities. Finally, the product was lyophilized overnight. The O-MoS_2 catalysts without the addition of GO power were also prepared using the above-procedure. For the thermostability investigation, the O-MoS_2/rGO catalysts were annealed at 500 or 800 °C for 2 h in argon atmosphere at a heating rate of 5 °C/min and cooled naturally.

In order to probe into the effect of DMF amount on the oxygen incorporation, morphology and crystal structure of O-MoS_2/rGO, a mixed solvent (10 mL in deionized water) containing different amounts of DMF (2 mL, 25 μL, 0.2 μL, and 0 μL) was also used in the hydrothermal reaction.

2.2. Preparation of Pristine, Undoped MoS_2/rGO Catalysts in Pure Deionized Water. In order to explore the oxygen incorporation mechanism, the solvent used in the reaction was changed to pure deionized water. Briefly, 10 mg freeze-dried GO power was dispersed in 10 mL deionized water, mixed with 20 mg of $(NH_4)_2MoS_4$ and 50 μL of reductant (hydrazine hydrate, N_2H_4) under sonication. The mixture was then transferred to a 25 mL Teflon-lined autoclave and kept in an oven at 190 °C for 15 h. The black product was collected and lyophilized overnight for use.

2.3. Preparation of Mechanical Mixture of O-MoS_2 and rGO. In order to investigate the synergistic effect between MoS_2 and rGO, pure rGO was prepared by a similar procedure except for the adding of $(NH_4)_2MoS_4$ precursors. The mechanical mixture of O-MoS_2 and rGO with a mass ratio of 7:3 (which was obtained from the results of thermal gravimetric analysis (TGA) of O-MoS_2/rGO) was prepared by mechanical ultrasonic treatment for 1 h.

2.4. Characterization. The morphologies and structures of catalysts were recorded on a Field emission scanning electron microscope (FESEM, Hitachi S4800) and a Transmission electron microscopy (TEM, Hitachi H-7650) equipped with an energy-dispersive X-ray spectroscopy (EDS) at an operating voltage of 200 kV. High-resolution TEM (HRTEM) images were observed at an operating voltage of 300 kV. The crystalline structures of catalysts were obtained on a X-ray diffractometer (Bruker AXS D8) using the Cu Ka radiation (λ = 0.15418 nm) with the 2θ scan from 5° to 80° at a step of 0.02°. The X-ray photoelectron spectroscopy (XPS) was collected by a KRATOS AXIS ULTRA-DLD with the binding energy calibrated by C 1s as reference energy (C 1s = 284.6 eV). Raman spectra were recorded on a Thermo Fisher DXR Raman spectrometer using a He−Ne laser (λ = 632.8 nm). The electrical conductivity of catalyst films were measured using a standard four-point-probe system by a Keithley 2400 instrument. The TGA was conducted on a TA Q500 Instrument under flowing air at a heating rate of 10 °C min^{-1}.

All electrochemical measurements were conducted on a CHI 660D electrochemical workstation (Shanghai Chenhua Instrument Co., China) in a three-electrode cell at room temperature. A glassy carbon electrode (GCE with the diameter of 3 mm) was used as the working electrode. A saturated calomel

DOI: 10.1021/acsami.6b06031
ACS Appl. Mater. Interfaces 2016, 8, 25210−25218

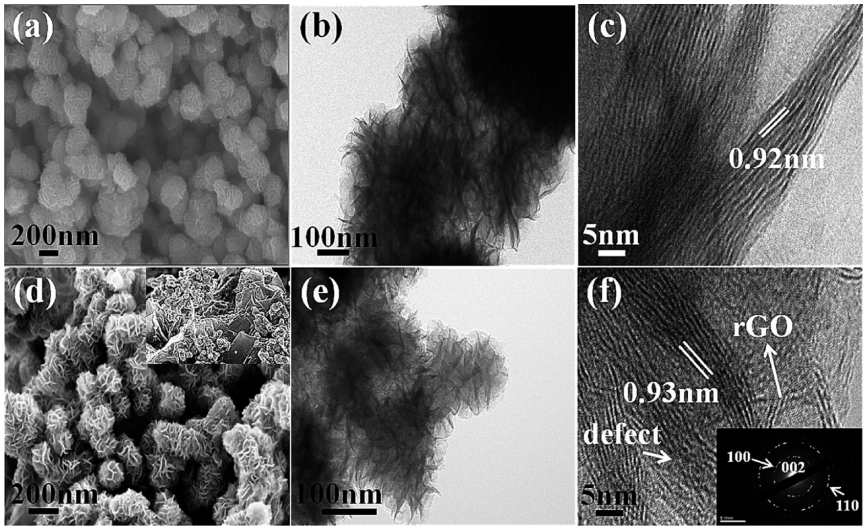

Figure 1. (a) SEM, (b) TEM, and (c) HRTEM images of 3D, vertically aligned O-MoS_2 nanosheets (no addition of GO). (d) SEM, (e) TEM, and (f) HRTEM images of O-MoS_2 nanosheets anchored on rGO. The inset in (d) is the low-resolution SEM image. The inset in (f) is the SAED pattern.

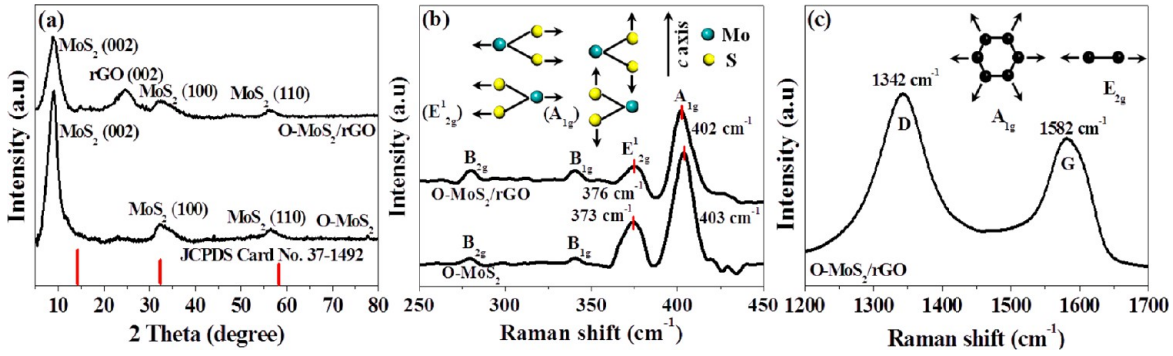

Figure 2. (a) XRD pattern and (b)-(c) Raman shift of vertically aligned O-MoS_2/rGO hybrid and pure O-MoS_2.

electrode (SCE) and a graphite rod were used as the reference electrode and counter electrode, respectively. For electrode preparation, 3 mg of the catalyst power and 120 μL Nafion solution (5 wt %) were dispersed in a 1.5 mL water−ethanol solution with volume ratio of (3:1) and sonicated for 0.5 h to form a homogeneous ink. Then 5 μL of the suspension (containing 9.25 μg of catalyst) was drop-casted onto the GCE surface (loading ca. 0.13 mg·cm^{-2}). Linear sweep voltammetry (LSV) measurement with a scan rate of 5 mV/s was conducted in a 0.5 M H_2SO_4 (purged in pure N_2 for 30 min before activity test). The electrochemical stability of the catalyst was evaluated by cycling the electrode for 2000 times with each cycle started at +0.10 V and ended at −0.3 V with a scan rate of 100 mV/s. AC electrochemical impedance spectroscopy (EIS) measurements were carried out in the same configuration at an overpotential of 0.165 V and a frequency range from 10^5 Hz to 0.1 Hz with an AC voltage of 5 mV. Double-layer capacitance (C_{dl}) and turnover frequency (TOF) were calculated according to the methods reported previously.[6,10] All the potentials were calibrated to RHE according to the previous literature.[17] The potential transfer from SCE to RHE was obtained according to the following equation: E(RHE) = E(SCE) + 0.267 V (Figure S1). Current density referring to the geometric surface area of the GCE was used.

3. RESULTS AND DISCUSSION

3.1. Microstructure of O-MoS_2 and O-MoS_2/rGO Catalysts. The formation of 2H-MoS_2 (both with and without addition of GO) was initially confirmed by our characterizations. The formed O-MoS_2 (no GO added) is 3D flower-like with a size around 100−200 nm (Figure 1a). No obvious morphology changes of the O-MoS_2 upon the addition of GO (Figure 1d), but O-MoS_2 are uniformly decorated on rGO sheets (inset in Figure 1d). These nanoflowers are composed by self-assembled ultrathin MoS_2 nanosheets with interconnected ripples and corrugations (Figure 1b and e). The HRTEM images of typical nanoflowers suggest a building structure of O-MoS_2 thin as <10 layers with crystal dislocations and defects (Figure 1c and f). The O-MoS_2 prepared with this route has interlayer spaces around 0.9 nm which is evidently larger than that of pure 2H-MoS_2 (~0.61 nm). The selected area electron diffraction (SAED) pattern (inset in Figure 1f) indicates that the as-prepared sample is a pure hexagonal phase with inhomogeneous crystal grain sizes due to the relative low crystallinity.[18,43] The enlargement of the interlayer distance of O-MoS_2 sheets is further confirmed by the XRD pattern (002 diffraction peak shifts to 9.1°, Figure 2a) when compared to bulk MoS_2 (2H-MoS_2, JCPDS 37-1492) with the 002 diffraction peak located at 14.2°.[6,14,35,44] The broad peak at approximating to 23.9° suggests the formation of stacked rGO nanosheets and the successful reduction from GO to rGO after

DOI: 10.1021/acsami.6b06031
ACS Appl. Mater. Interfaces 2016, 8, 25210−25218

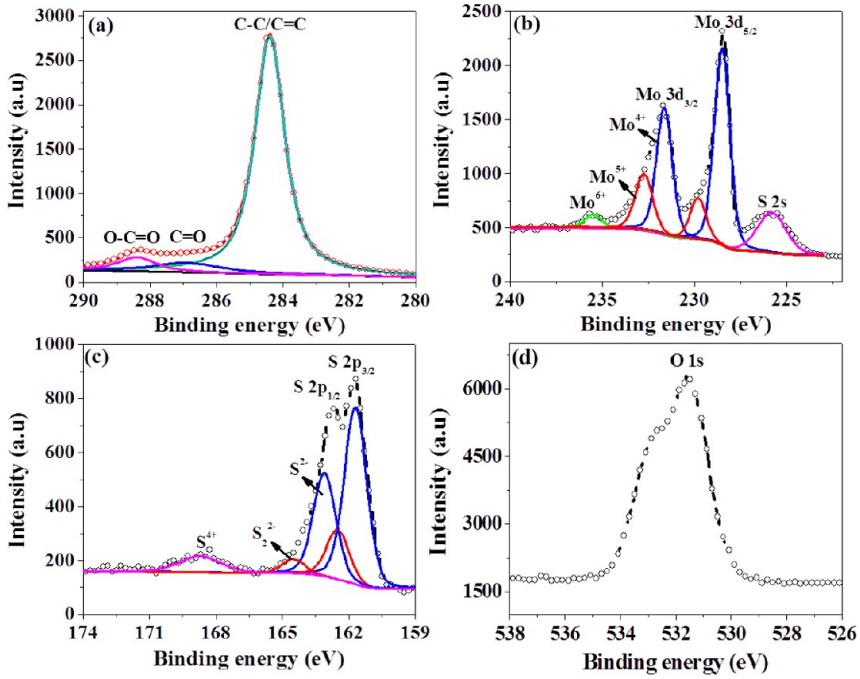

Figure 3. XPS spectra of vertically aligned O-MoS_2/rGO hybrid: (a) C 1s, (b) Mo 3d, (c) S 2p, and (d) O 1s.

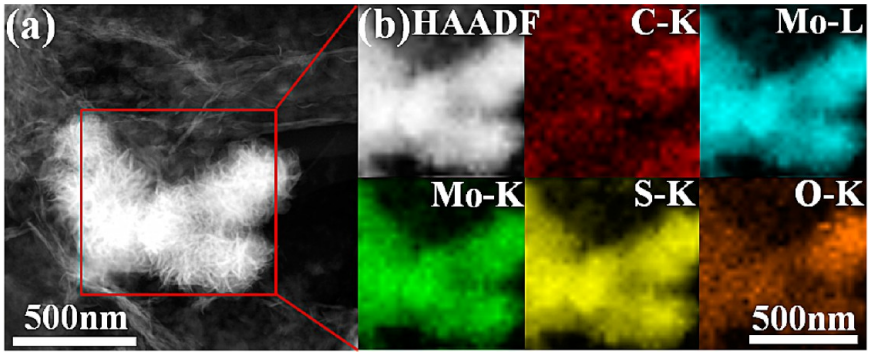

Figure 4. (a) TEM, (b) high-annular dark-field scanning TEM image (HAADF-STEM) and corresponding element mapping images of O-MoS_2/rGO hybrid, indicating the homogeneous distribution of C, Mo, S, and O.

hydrothermal process (Figure S2a).[45] The Raman spectrum in Figure 2b reveals two dominant peaks located at 373 and 403 cm^{-1} which could be assigned to the characteristic peaks of in-plane E^1_{2g} and out-of-plane A_{1g} along the *c*-axis vibrational modes of hexagonal MoS_2 (Mo−S bonds).[18] The peak intensity related to A_{1g} vibrational mode is about three times larger than that related to E^1_{2g} one. Additionally, the wide peak related to E^1_{2g} vibrational mode is responsible for the poor crystallization and rich defects along the 002 crystal planes,[19] as seen in Figure 1c and f. Previous studies confirmed that the frequency difference between the two peaks presented the number variation of (002) crystal-plane layers along the *c*-axis of MoS_2 nanosheets.[27,29] Our results show that the differences between the two dominant peaks are 30 and 26 cm^{-1} for O-MoS_2 and O-MoS_2/rGO, respectively. This could be attributed to the fact that the GO can effectively prevent MoS_2 nanosheets from stacking during the hydrothermal process.[43,46] The peaks at 281 and 340 cm^{-1} can be identified as the B_{2g} and B_{1g} vibrational modes (Mo−O bonds), confirming the successful oxygen incorporation in the MoS_2.[6] The characteristic peaks at 1342 and 1582 cm^{-1} for rGO in Figure 2c can be ascribed to D band (represents edges, disordered carbon and defects) and G band (corresponds to vibration of ordered sp^2-hybrided carbon).[47] The intensity ratios for I_D/I_G are 1.40 and 0.97 (Figure S2b) for rGO and GO, respectively, suggesting the partially destroyed delocalized π conjugation[48] during the hydrothermal process and the successful reduction from GO to rGO.

XPS was used to illustrate the atomic valence states of elements in the hybrids. Figure 3 shows the XPS core-level spectra of the prepared O-MoS_2/rGO, giving peaks of C, Mo, S, and O (corresponding to EDS mapping during TEM characterization in Figure 4) and the atomic percentages (e.g., C = 58.12, O = 13.11, Mo = 8.54, and S = 20.23 at. %). In compare with the XPS results of pure rGO (C = 83.82 and O = 16.18 at. %) and O-MoS_2 (O = 6.30, Mo = 27.65 and S = 66.05 at. %), we suggest the ratio of Mo/S/O in O-MoS_2 is about 1/2.4/0.23 (e.g., $O_{0.23}$-$MoS_{2.4}$ or $O_{0.23}$-$MoS_{2.4}$/rGO). This excess sulfur atoms might be regarded as uncoordinated sulfur atoms with negative charges, which could facilitate proton adsorption and conversion into H_2.[22,25] The chemical reduction of GO by DMF has been well recognized.[49] In compare with the XPS result of GO (Figure S2c), the O-related signal in the C 1s of rGO (e.g., C−O, C═O, and O−C═O groups) is highly decreased (Figure 3a), suggesting that GO has been reduced to

DOI: 10.1021/acsami.6b06031
ACS Appl. Mater. Interfaces 2016, 8, 25210−25218

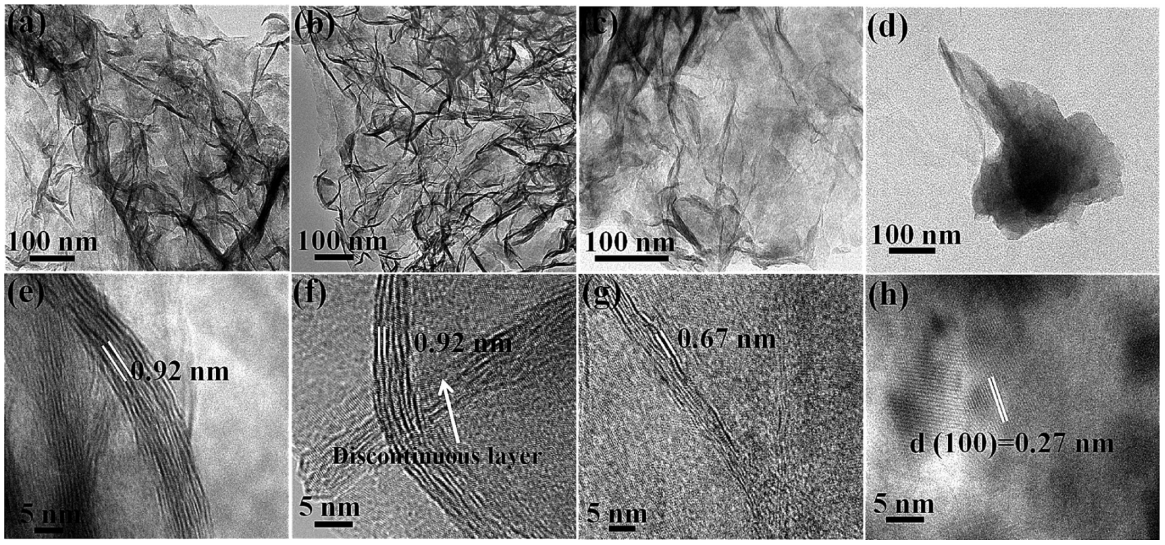

Figure 5. (a)−(d) SEM images and (e)−(h) corresponding TEM images of MoS_2/rGO catalysts synthesized with various amounts of DMF in the mixed solvent (10 mL): (a,e) 2 mL, (b,f) 25 μL, (c,g) 0.2 μL, (d,h) 0 μL, respectively.

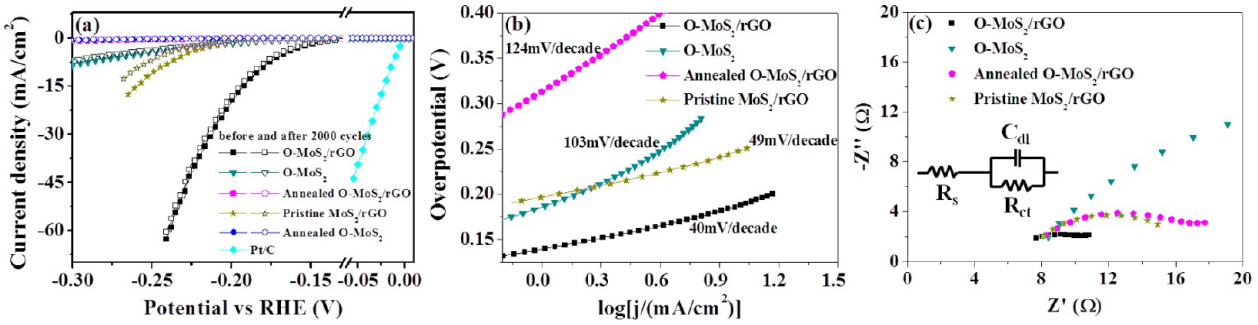

Figure 6. (a) Polarization curves and durability tests for various MoS_2/rGO catalysts in a 0.5 M H_2SO_4 solution at a scan rate of 100 mV/s in the potential range from −0.3 to 0.1 V. (b) Corresponding Tafel slopes of various MoS_2/rGO catalysts in a N_2-saturated 0.5 M H_2SO_4 solution at a scan rate of 5 mV/s. (c) AC impedance spectra of various MoS_2/rGO catalysts in a 0.5 M H_2SO_4 solution with the frequency range from 10^5 to 0.1 Hz and an amplitude of 5.0 mV. The inset is the equivalent model of system.

certain extent. We further performed this reduction reaction without the addition of $(NH_4)_2MoS_4$ precursor as control (the O doping of MoS_2 from GO is not the case), and the XPS result suggested that the DMF acted as a reducing agent to reduce GO in above reactions (Figure S2c). This is in agreement with the results of XRD and Raman measurements for pure rGO (Figure S2a and b). XPS analysis of the sample also suggests that the prepared MoS_2 (both the Mo and S) for O-MoS_2/rGO are slightly oxidized, giving oxidized Mo 3d and S 2p peaks at around 235.6 and 168.7 eV,[18] respectively, except the observation of typical binding energies of 2H-MoS_2 (231.7 (Mo 3d3/2), 228.5 (Mo 3d1/2), 162.6 (S 2p1/2), and 161.8 eV (S 2p3/2) in Figure 3b and c).[4,10] These oxidization states are considered to responsible for the enlargement of the interlayer distance of thin MoS_2 sheets, and occurred even without the existence of GO (Figure S3a and b). The peaks at 163.8 ± 0.1 eV and 164.8 ± 0.1 eV reflect the bridging S_2^{2-} ligand or the aspical S^{2-} one, which steps from the unsaturated (uncoordinated) S atoms.[10,33] The peak related to S^{4+} (168.7 eV) might be attributed to the existence of sulfate groups.[18] The peak located at 531.5 ± 0.1 eV in the O 1s core-level spectrum (Figure 3d) could be assigned to the incorporation of oxygen into MoS_2,[6,14,40] leading to the expansion of layer distance,[6] which is in good accordance with the observation shown in Figure 1f. Moreover, almost same chemical states for Mo, S, and O elements are observed in O-MoS_2 (Figure S3), indicating that the oxygen incorporation process indeed happens even without the existence of GO.

3.2. Effect of Addition Amounts of DMF on Crystal Structure of O-MoS_2 Catalysts. To better explore the origin of incorporated oxygen in the O-MoS_2/rGO hybrids, controllable experiments were designed. With the gradient decrease of DMF from initial 10 mL (for O-MoS_2/rGO preparation) to 25 μL in the mixed solvent (10 mL), the vertically aligned flower-like morphology vanishes, while the distance of 002 crystal planes still remains 0.92 nm (Figure 5a and b, e and f). Further decrease of DMF down to 0.2 and 0 μL, disordered and discontinuous MoS_2 nanosheets with the interlayer distances of 0.67 nm (Figure 5c and g) and even amorphous structure (Figure 5d and h) could be obtained due to the lack of reduction agent.

We synthesized O-MoS_2 catalysts with same procedure of O-MoS_2/rGO but without adding GO power. The XRD (Figure 2a), Raman (Figure 2b), and XPS measurement (Figure S3) of this O-MoS_2 are nearly the same to the above O-MoS_2/rGO (Figure 2a, Figure 2b, and Figure 3; MoS_2 was oxidized with similar extent in both cases with and without addition of GO), suggesting that the oxidization of MoS_2 is mainly due to the DMF. Moreover, we further replaced DMF solvent with pure deionized water to prepare MoS_2/rGO (with the addition of 50

DOI: 10.1021/acsami.6b06031
ACS Appl. Mater. Interfaces 2016, 8, 25210−25218

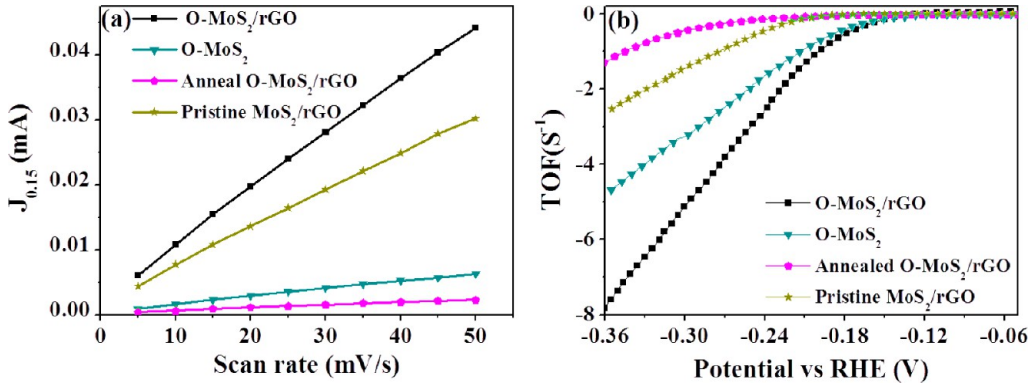

Figure 7. (a) Relations of difference between anodic and cathodic currents at 0.15 V (vs RHE) ($J_{0.15} = J_a$-J_c) with various scan rates from 5 to 50 mV/s. The slope is double C_{dl}. (b) Turnover frequency (TOF) of various MoS_2/rGO catalysts in a 0.5 M H_2SO_4 solution at a scan rate of 50 mV/s.

μL N_2H_4 as reduction agent), and the interlayer space of the resultant MoS_2 restored to ~0.67 nm (Figure S4c) with a related XRD peak at 13.8° (Figure S4d). Our above investigations have suggested that the interlayer spaces of MoS_2 should be enlarged with the oxidization (Figure 1c and Figure 1f). All these information suggest that the O dopants of MoS_2 (in O-MoS_2/rGO) are mainly from DMF, and that from GO or oxygen-containing precursors are likely few, which is different from previous reports.[14,40] Inspired by the above experiment results, we assume the role of DMF solvent in the O-MoS_2/rGO synthesis process as following. DMF first served as the reduction agent to produce MoS_2 nanosheets, then additional DMF worked as oxygen donor for oxygen-atom incorporating into the MoS_2 nanosheets. Furthermore, the incorporated oxygen was easily removed from the MoS_2 structures after annealing at 500 or 800 °C. The flower-like morphology of MoS_2 remains (Figure S5a and b, d and e) but the interlayer distance decreases to 0.67 nm (Figure S5c) or 0.65 nm (Figure S5f) after heat treatment. This is reasonable as the successful removal of incorporated oxygen during heat treatment,[50] resulting in the decrease of distance of 002 crystal planes and the improvement of crystalline quality,[4,19] as deduced from the narrower peak related to E^1_{2g} vibrational mode and redshift of diffraction peaks assigned to the (002) crystal plane of MoS_2 (Figure S6).

3.3. Electrochemical Behaviors of O-MoS_2/rGO Catalysts. The electrochemical performances of various catalysts were investigated in a N_2-saturated 0.5 M H_2SO_4 solution by using a three-electrode setup. As shown in Figure 6a, with same amount (0.13 mg·cm^{-2}) catalyst immobilized on GCE, the O-MoS_2/rGO hybrid has the smallest onset overpotential (~100 mV vs RHE obtained at 0.1 mA/cm^2) compared to O-MoS_2 and other MoS_2/rGO hybrids (also see Table S1). This overpotential is much smaller than that of defect-rich MoS_2 ultrathin nanosheets (onset overpotential 120 mV) and many other MoS_2 based catalysts (Figure S7).[1,4−6,21,38,51−57] We achieved a current density of 20 mA/cm^2 (at 200 mV vs RHE), which is 13.2 times larger than that without GO and 16.4 times larger than that of pristine MoS_2/rGO catalyst. Tafel slope of the O-MoS_2/rGO is shown in Figure 6b, suggesting a highly efficient catalytic performance with a small slope around 40 mV/decade (lower than many reported MoS_2-based catalysts in Figure S7),[1,4−6,21,38,51−57] and the Volmer-Heyovsky mechanism associated with electrochemical desorption step as the rate-limiting step.[1,5,51] The durability test for O-MoS_2/rGO catalyst indicates that only 1.3% loss in the current density even after continuous 2000 cycles (Figure 6a), without any clear morphology and element constituent changes (Figure S8). Such excellent HER performance of O-MoS_2/rGO catalysts could be rationalized as follows: (i) the incorporated oxygen from DMF solvent improves the intrinsic conductivity (the resistivities of O-MoS_2/rGO, pristine MoS_2/rGO, and annealed O-MoS_2/rGO catalyst films spin-coated on SiO_2/Si substrates obtained by four-point-probe system are 3.3×10^{-2} Ω·cm, 0.25 Ω·cm, and 0.12 Ω·cm, respectively), promoting fast mobility of the electron along the MoS_2 nanosheets;[7,40] (ii) oxygen incorporation increases the defect and vertical edge ratio, giving more exposed Mo and S edges to participate catalytic process;[58] (iii) in situ synthesis of O-MoS_2/rGO through hydrothermal method results in the pronounced synergetic effect between MoS_2 nanosheets and rGO with better mechanical adhesion and stability (see Supporting Information on the electrochemical behavior of mechanical mixture of O-MoS_2 and rGO in Figure S9). The addition of DMF promotes the reduction of GO, which may also increase the catalytic performance. The decisive influence of oxygen incorporation on the HER catalytic activity is further confirmed by annealing the O-MoS_2/rGO hybrids at 500 °C (Figure 6a and b). Upon the annealing of the catalyst, the incorporated oxygen gradually losses, associated with the interlayer space of MoS_2 sheets (0.93 nm) restoring to that of pure 2H-MoS_2 (~0.67 nm) (Figure S5c). The microstructure of annealed sample is different to that of pristine MoS_2/rGO. Compared with the pristine MoS_2/rGO, the annealed O-MoS_2/rGO has more MoS_2 layers with less crystal dislocations and defects (Figure S4c and Figure S5c). The Raman and XRD data (Figure S6a and b) also suggest that the crystallization of MoS_2 is improved by the annealing. Since HER of MoS_2 is highly depend on the edge ratio, exposed defect site on the basal plane, and electron hopping efficiency (electrical conductivity can be largely reduced with each addition of layer),[13] the annealing increases the crystallization, in turn, reduces the number of catalytically active sites and electrical conductivity. This makes the HER performances between the annealed sample and pristine MoS_2/rGO are so significantly different. We also performed the EIS of the catalysts at the overpotential of 165 mV to explore the kinetics during the HER process. The O-MoS_2/rGO catalyst shows the smallest R_{ct} about 3 Ω, which increases upon the annealing, or without rGO support (Figure 6c), and evidently confirms that both oxygen incorporation and rGO hybrid structure increase charge transfer of the catalyst for HER.

DOI: 10.1021/acsami.6b06031
ACS Appl. Mater. Interfaces 2016, 8, 25210−25218

Furthermore, the electrochemical area is regarded as another effective way to estimate the catalytic activity of material.[4,6,7] The double layer capacitance (C_{dl}) which characterizes effective active surface area (EASA) and rich exposed active sites[12,33] are also calculated according to the cyclic voltammetry measurement (Figure S10 for more information). From the relations of difference between anodic and cathodic currents at 0.15 V (vs RHE) ($J_{0.15} = J_a - J_c$) with various scan rates from 5 to 50 mV/s (Figure 7a), the O-MoS_2/rGO catalyst exhibits the largest slopes (C_{dl} = 5.98 mF/cm^2) than other MoS_2/rGO catalysts (Table S1), and this value is rather competitive considering the low mass loading when compared to previously reported MoS_2-based catalysts (Figure S7).[6,21,54] We then further compared the Turnover frequency (TOF) of different catalysts, which is an effective way to determine the active sites of the catalyst[10,16] (Figure S11 for more information). The calculated TOF for O-MoS_2/rGO catalyst is 1.74, 5.15, and 7.37 s^{-1} at the overpotential of 220, 300, and 350 mV, respectively, which is much higher than those of our prepared O-MoS_2 (3.24 s^{-1} at η = 300 mV) and pristine MoS_2/rGO (1.47 s^{-1} at η = 300 mV) catalysts (Table S1) and those of MoS_2-based catalysts, such as defect-rich ultrathin MoS_2 nanosheets[4] (0.70 s^{-1} at η = 300 mV), amorphous MoS_2 films (0.80 s^{-1} at η = 220 mV)[51] and 3D MoS_2 nanospheres (0.89 s^{-1} at η = 350 mV).[57] Although pristine MoS_2/rGO has lower TOF than O-MoS_2, it exhibits better catalytic ability (Figure 6) due to the various exposed vertically aligned edges. The TOF only represents the catalytic ability of each active site. It is reasonable to find that the TOF of O-MoS_2 is higher than pristine MoS_2/rGO due to the O-related defect level. Nevertheless, catalytic performance of MoS_2 is also affected by the number of active site, and the electrical conductivity between catalyst and electrode. The vertically aligned MoS_2 on rGO has much more exposed active sites for HER, and the rGO bonds the electrode to provide better electrical transport between catalyst and electrode, which offers the MoS_2/rGO with better overall catalytic performance.

4. CONCLUSIONS

In conclusion, we have demonstrated a facile way to fabricate vertically aligned O-MoS_2/rGO (O-incorporated MoS_2 anchored on rGO sheet) catalyst with expanded layer distance of 002 crystal planes. Controlled synthesis has been designed to explore the mechanism of oxygen incorporation. We found that DMF first served as the reducing agent and then acted as oxygen-element donor to enlarge the layer-to-layer distance of MoS_2 nanosheets. The as-prepared O-MoS_2/rGO catalyst exhibited excellent HER activity with a small onset overpotential of 100 mV, a large current density of 20 mA/cm^2 at 200 mV, a small Tafel slope as low as 40 mV/decade, and superior stability even after 2000 continuous scans. What is more astonishing is that the dominant Turnover frequency (5.15 s^{-1} at 300 mV) and high double layer capacitance (5.98 mF/cm^2) can be obtained considering the low mass loading when compared to previously reported MoS_2-based catalysts. Such highly efficient HER could be attributed to not only the enhanced intrinsic conductivity and vertical edge ratio of MoS_2 with oxygen incorporation, but also the superior stability and accelerated charge transfer process due to the synergetic effect between MoS_2 and rGO. This research proposes a new perspective to open a new strategy to synthesize other transition metal sulfides with excellent HER performance.

ASSOCIATED CONTENT

Supporting Information

The Supporting Information is available free of charge on the ACS Publications website at DOI: 10.1021/acsami.6b06031.

Details of the structures and electrochemical performances (PDF)

AUTHOR INFORMATION

Corresponding Author

*E-mail: liuaiping1979@gmail.com.

Author Contributions

A.L. proposed the research and experiment; L.Z. and J.Z. assisted the main experimental works to achieve the research vision; H.W. assisted the measurements; L.L. provided expertise suggestion to the experimental work and assisted with the manuscript drafting.

Notes

The authors declare no competing financial interest.

ACKNOWLEDGMENTS

This work was supported by the National Natural Science Foundation of China (Nos. 51272237, 51572242 and 11372280), the Zhejiang Provincial Natural Science Foundation of China (No. LY16E020011), the 521 Talent Project of Zhejiang Sci-Tech University, the Program for Innovative Research Team of Zhejiang Sci-Tech University (No. 15010039-Y) and the Opening Fund of State Key Laboratory of Nonlinear Mechanics.

REFERENCES

(1) Li, Y. G.; Wang, H. L.; Xie, L. M.; Liang, Y. Y.; Hong, G. S.; Dai, H.J. MoS_2 Nanoparticles Grown on Graphene: an Advanced Catalyst for the Hydrogen Evolution Reaction. *J. Am. Chem. Soc.* **2011**, *133*, 7296−7299.

(2) Laursen, B.; Kegnaes, S.; Dahl, S.; Chorkendorff, I. Molybdenum Sulfides-Efficient and Viable Materials for Electro- and Photoelectrocatalytic Hydrogen Evolution. *Energy Environ. Sci.* **2012**, *5*, 5577−5591.

(3) Jaramillo, T. F.; Jorgensen, K. P.; Bonde, J.; Nielsen, J. H.; Horch, S.; Chorkendorff, I. Identification of Active Edge Sites for Electrochemical H_2 Evolution from MoS_2 Nanocatalysts. *Science* **2007**, *317*, 100−102.

(4) Xie, J. F.; Zhang, H.; Li, S.; Wang, R. X.; Sun, X.; Zhou, M.; Zhou, J. F.; Lou, X. W.; Xie, Y. Defect-Rich MoS_2 Ultrathin Nanosheets with Additional Active Edge Sites for Enhanced Electrocatalytic Hydrogen Evolution. *Adv. Mater.* **2013**, *25*, 5807−5813.

(5) Chang, Y. H.; Lin, C. T.; Chen, T. Y.; Hsu, C. L.; Lee, Y. H.; Zhang, W. J.; Wei, K. H.; Li, L. J. Highly Efficient Electrocatalytic Hydrogen Production by MoS_x Grown on Graphene-Protected 3D Ni Foams. *Adv. Mater.* **2013**, *25*, 756−760.

(6) Xie, J. F.; Zhang, J. J.; Li, S.; Grote, F. B.; Zhang, X. D.; Wang, R. X.; Zhang, H.; Lei, Y.; Pan, B. C.; Xie, Y. Controllable Disorder Engineering in Oxygen-Incorporated MoS_2 Ultrathin Nanosheets for Efficient Hydrogen Evolution. *J. Am. Chem. Soc.* **2013**, *135*, 17881−17888.

(7) Lukowski, M. A.; Daniel, A. S.; Meng, F.; Forticaux, A.; Li, L. S.; Jin, S. Enhanced Hydrogen Evolution Catalysis from Chemically Exfoliated Metallic MoS_2 Nanosheets. *J. Am. Chem. Soc.* **2013**, *135*, 10274−10277.

(8) Wang, T. T.; Zhuo, J. Q.; Du, K. Z.; Chen, B. B.; Zhu, Z. W.; Shao, Y. H.; Li, M. X. Electrochemically Fabricated Polypyrrole and MoS_x Copolymer Films as a Highly Active Hydrogen Evolution Electrocatalyst. *Adv. Mater.* **2014**, *26*, 3761−3766.

DOI: 10.1021/acsami.6b06031
ACS Appl. Mater. Interfaces 2016, 8, 25210−25218

(9) Kibsgaard, J.; Chen, Z. B.; Relnecke, B. N.; Jaramillo, T. F. Engineering the Surface Structure of MoS_2 to Preferentially Expose Active Edge Sites for Electrocatalysis. *Nat. Mater.* **2012**, *11*, 963−969.
(10) Yan, Y.; Xia, B. Y.; Ge, X. M.; Liu, Z. L.; Wang, J. Y.; Wang, X. Ultrathin MoS_2 Nanoplates with Rich Active Sites as Highly Efficient Catalyst for Hydrogen Evolution. *ACS Appl. Mater. Interfaces* **2013**, *5*, 12794−12798.
(11) Wu, Z. Z.; Fang, B. Z.; Wang, Z. P.; Wang, C. L.; Liu, Z. H.; Liu, F. F.; Wang, W.; Alfantazi, A.; Wang, D. Z.; Wilkinson, D. P. MoS_2 Nanosheets: A Designed Structure with High Active Site Density for the Hydrogen Evolution Reaction. *ACS Catal.* **2013**, *3*, 2101−2107.
(12) Wang, H. T.; Lu, Z. Y.; Kong, D. S.; Sun, J.; Hymel, T. M.; Cui, Y. Electrochemical Tuning of MoS_2 Nanoparticles on Three-Dimensional Substrate for Efficient Hydrogen Evolution. *ACS Nano* **2014**, *8*, 4940−4947.
(13) Yu, Y. F.; Huang, S. Y.; Li, Y. P.; Steinmann, S. N.; Yang, W. T.; Cao, L. Y. Layer-Dependent Electrocatalysis of MoS_2 for Hydrogen Evolution. *Nano Lett.* **2014**, *14*, 553−558.
(14) Zhou, W. J.; Zhou, K.; Hou, D. M.; Liu, X. J.; Li, G.Q.; Sang, Y. H.; Liu, H.; Li, L. G.; Chen, S. W. Three-Dimensional Hierarchical Frameworks Based on MoS_2 Nanosheets Self-Assembled on Graphene Oxide for Efficient Electrocatalytic Hydrogen Evolution. *ACS Appl. Mater. Interfaces* **2014**, *6*, 21534−21540.
(15) Hou, Y.; Zhang, B.; Wen, Z. H.; Cui, S. M.; Guo, X. R.; He, Z.; Chen, J. H. A 3D Hybrid of Layered MoS_2/Nitrogen-doped Graphene Nanosheet Aerogels: An Effective Catalyst for Hydrogen Evolution in Microbial Electrolysis Cells. *J. Mater. Chem. A* **2014**, *2*, 13795−13800.
(16) Merki, D.; Fierro, S.; Vrubel, H.; Hu, X. L. Amorphous Molybdenum Sulfide Films as Catalysts for Electrochemical Hydrogen Production in Water. *Chem. Sci.* **2011**, *2*, 1262−1267.
(17) Kiran, V.; Mukherjee, D.; Jenjeti, R. N.; Sampath, S. Active Guests in the MoS_2/$MoSe_2$ Host Lattice: Efficient Hydrogen Evolution using Few-Layer Alloys of $MoS_{2(1-x)}Se_{2x}$. *Nanoscale* **2014**, *6*, 12856−12863.
(18) Zhang, X. L.; Xu, J. B.; Yan, K. Y.; Wang, H.; Wang, Z. L.; Yang, S. H. Space-Confined Growth of MoS_2 Nanosheets within Graphite: The Layered Hybrid of MoS_2 and Graphene as an Active Catalyst for Hydrogen Evolution Reaction. *Chem. Mater.* **2014**, *26*, 2344−2353.
(19) Yan, Y.; Ge, X. M.; Liu, Z. L.; Wang, J. Y.; Lee, J. M.; Wang, X. Facile Synthesis of Low Crystalline MoS_2 Nanosheet-Coated CNTs for Enhanced Hydrogen Evolution Reaction. *Nanoscale* **2013**, *5*, 7768−7771.
(20) Benck, J. D.; Hellstern, T. R.; Kibsgaard, J.; Chakthannont, P.; Jaramillo, T. F. Catalyzing the Hydrogen Evolution Reaction (HER) with Molybdenum Sulfide Nanomaterials. *ACS Catal.* **2014**, *4*, 3957−3971.
(21) Deng, Z. H.; Li, L.; Ding, W.; Xiong, K.; Wei, Z. D. Synthesized Ultrathin MoS_2 Nanosheets Perpendicular to Graphene for Catalysis of Hydrogen Evolution Reaction. *Chem. Commun.* **2015**, *51*, 1893−1896.
(22) Li, D. J.; Maiti, U. N.; Lim, J.; Choi, D. S.; Lee, W. J.; Oh, Y.; Lee, G. Y.; Kim, S. O. Molybdenum Sulfide/N-Doped CNT Forest Hybrid Catalysts for High-Performance Hydrogen Evolution Reaction. *Nano Lett.* **2014**, *14*, 1228−1233.
(23) Zhao, Y. F.; Xie, X. Q.; Zhang, J. Q.; Liu, H.; Ahn, H. J.; Sun, K. N.; Wang, G. X. MoS_2 Nanosheets Supported on 3D Graphene Aerogel as a Highly Efficient Catalyst for Hydrogen Evolution. *Chem. - Eur. J.* **2015**, *21*, 15908−15913.
(24) Worsley, M. A.; Shin, S. J.; Merrill, M. D.; Lenhardt, J.; Nelson, A. J.; Woo, L. Y.; Gash, A. E.; Baumann, T. F.; Orme, C. A. Ultralow Density, Monolithic WS_2, MoS_2, and MoS_2/Graphene Aerogels. *ACS Nano* **2015**, *9*, 4698−4705.
(25) Merki, D.; Vrubel, H.; Rovelli, L.; Fierro, S.; Hu, X. L. Fe, Co, and Ni Ions Promote the Catalytic Activity of Amorphous Molybdenum Sulfide Films for Hydrogen Evolution. *Chem. Sci.* **2012**, *3*, 2515−2525.
(26) Hinnemann, B.; Moses, P. G.; Bonde, J.; Jorgensen, K. P.; Nielsen, J. H.; Horch, S.; Chorkendorff, I.; Norskov, J. K. Biomimetic Hydrogen Evolution: MoS_2 Nanoparticles as Catalyst for Hydrogen Evolution. *J. Am. Chem. Soc.* **2005**, *127*, 5308−5309.
(27) Kong, S.; Wang, H. T.; Cha, J. J.; Pasta, M.; Koski, K. J.; Yao, J.; Cui, Y. Synthesis of MoS_2 and $MoSe_2$ Films with Vertically Aligned Layers. *Nano Lett.* **2013**, *13*, 1341−1347.
(28) Shi, J. P.; Ma, D. L.; Han, G. F.; Zhang, Y.; Ji, Q. Q.; Gao, T.; Sun, J. Y.; Song, X. J.; Li, C.; Zhang, Y. S.; Lang, X. Y.; Zhang, Y. F.; Liu, Z. F. Controllable Growth and Transfer of Monolayer MoS_2 on Au Foils and Its Potential Application in Hydrogen Evolution Reaction. *ACS Nano* **2014**, *8*, 10196−10204.
(29) Wang, H. T.; Lu, Z. Y.; Xu, S. C.; Kong, D. S.; Cha, J. J.; Zheng, G. Y.; Hsu, P. C.; Yan, K.; Bradshaw, D.; Prinz, F. B.; Cui, Y. Electrochemical Tuning of Vertically Aligned MoS_2 Nanofilms and Its Application in Improving Hydrogen Evolution Reaction. *Proc. Natl. Acad. Sci. U. S. A.* **2013**, *110*, 19701−19706.
(30) Ren, X. P.; Pang, L. Q.; Zhang, Y. X.; Ren, X. D.; Fan, H. B.; Liu, S. Z. One-Step Hydrothermal Synthesis of Monolayer MoS_2 Quantum Dots for Highly Efficient Electrocatalytic Hydrogen Evolution. *J. Mater. Chem. A* **2015**, *3*, 10693−10697.
(31) Zhang, J. M.; Zhao, L.; Liu, A. P.; Li, X. Y.; Wu, H. P.; Lu, C. D. Three-dimensional MoS_2/rGO Hydrogel with Extremely High Double-layer Capacitance as Active Catalyst for Hydrogen Evolution Reaction. *Electrochim. Acta* **2015**, *182*, 652−658.
(32) Yang, L. J.; Zhou, W. J.; Hou, D. M.; Zhou, K.; Li, G. Q.; Tang, Z. H.; Li, L. G.; Chen, S. W. Porous Metallic MoO_2-supported MoS_2 Nanosheets for Enhanced Electrocatalytic Activity in The Hydrogen Evolution Reaction. *Nanoscale* **2015**, *7*, 5203−5208.
(33) Benck, J. D.; Chen, Z. B.; Kurizky, L. Y.; Forman, A. J.; Jaramillo, T. F. Amorphous Molybdenum Sulfide Catalysts for Electrochemical Hydrogen Production: Insights into the Origin of their Catalytic Activity. *ACS Catal.* **2012**, *2*, 1916−1923.
(34) Vrubel, H.; Hu, X. L. Growth and Activation of an Amorphous Molybdenum Sulfide Hydrogen Evolving Catalyst. *ACS Catal.* **2013**, *3*, 2002−2011.
(35) Kong, H.; Cha, J. J.; Wang, H. T.; Lee, H. R.; Cui, Y. First-row Transition Metal Dichalcogenide Catalysts for Hydrogen Evolution Reaction. *Energy Environ. Sci.* **2013**, *6*, 3553−3558.
(36) Deng, J.; Li, H. B.; Xiao, J. P.; Tu, Y. C.; Deng, D. H.; Yang, H. X.; Tian, H. F.; Li, J.; Ren, P. Q.; Bao, X. H. Triggering The Electrocatalytic Hydrogen Evolution Activity of The Inert Two-dimensional MoS_2 Surface *via* Single-atom Metal Doping. *Energy Environ. Sci.* **2015**, *8*, 1594−1601.
(37) Wu, Z. Z.; Tang, C. Y.; Zhou, P.; Liu, Z. H.; Xu, Y. S.; Wang, D. Z.; Fang, B. Z. Enhanced Hydrogen Evolution Catalysis from Osmotically Swollen Ammoniated MoS_2. *J. Mater. Chem. A* **2015**, *3*, 13050−13056.
(38) Ren, X. P.; Fan, Q.; Ma, H. B.; Pang, L. Q.; Zhang, Y. X.; Yao, Y.; Ren, X. D.; Liu, S. Z. A Se-doped MoS_2 Nanosheet for Improved Hydrogen Evolution Reaction. *Chem. Commun.* **2015**, *51*, 15997−16000.
(39) Gong, Q. F.; Cheng, L.; Liu, C. H.; Zhang, M.; Feng, Q. L.; Ye, H. L.; Zeng, M.; Xie, L. M.; Liu, Z.; Li, Y. G. Ultrathin $MoS_{2(1-x)}Se_{2x}$ Alloy Nanoflakes For Electrocatalytic Hydrogen Evolution Reaction. *ACS Catal.* **2015**, *5*, 2213−2219.
(40) Guo, J. X.; Li, F. F.; Sun, Y. Y.; Zhang, X.; Tang, L. Oxygen-Incorporated MoS_2 Ultrathin Nanosheets Grown on Graphene for Efficient Electrochemical Hydrogen Evolution. *J. Power Sources* **2015**, *291*, 195−200.
(41) Zhao, X.; Zhu, H.; Yang, X. R. Amorphous Carbon Supported MoS_2 Nanosheets as Effective Catalysts for Electrocatalytic Hydrogen Evolution. *Nanoscale* **2014**, *6*, 10680−10685.
(42) Hummers, W. S., Jr; Offeman, R. E. Preparation of Graphitic Oxide. *J. Am. Chem. Soc.* **1958**, *80*, 1339−1339.
(43) Chang, K.; Chen, W. X. l-Cysteine-Assisted Synthesis of Layered MoS_2/Graphene Composites with Excellent Electrochemical Performances for Lithium Ion Batteries. *ACS Nano* **2011**, *5*, 4720−4728.
(44) Gao, M. R.; Chan, M. K. Y.; Sun, Y. G. Metal Organic Framework-mediated Synthesis of Highly Active and Stable Fischer−Tropsch Catalysts. *Nat. Commun.* **2015**, *6*, 1−8.

DOI: 10.1021/acsami.6b06031
ACS Appl. Mater. Interfaces 2016, 8, 25210−25218

(45) Ma, C. B.; Qi, X. Y.; Chen, B.; Bao, S. Y.; Yin, Z. Y.; Wu, X. J.; Luo, Z. M.; Wei, J.; Zhang, H. L.; Zhang, H. MoS_2 Nanoflower-decorated Reduced Graphene Oxide Paper for High-Performance Hydrogen Evolution Reaction. *Nanoscale* **2014**, *6*, 5624−5629.
(46) Liu, K. K.; Zhang, W. J.; Lee, Y. H.; Lin, Y. C.; Chang, M. T.; Su, C. Y.; Chang, C. S.; Li, H.; Shi, Y. M.; Zhang, H.; Lai, C. S.; Li, L. J. Growth of Large-Area and Highly Crystalline MoS_2 Thin Layers on Insulating Substrates. *Nano Lett.* **2012**, *12*, 1538−1544.
(47) Huang, G. C.; Chen, T.; Chen, W. X.; Wang, Z.; Chang, K.; Ma, L.; Huang, F. H.; Chen, D. Y.; Lee, J. Y. Graphene-Like MoS_2/Graphene Composites: Cationic Surfactant-Assisted Hydrothermal Synthesis and Electrochemical Reversible Storage of Lithium. *Small* **2013**, *9*, 3693−3703.
(48) Stankovich, S.; Dikin, D. A.; Piner, R. D.; Kohlhaas, K. A.; Kleinhammes, A.; Jia, Y.; Wu, Y.; Nguyen, S. T.; Ruoff, R. S. Synthesis of Graphene-based Nanosheets via Chemical Reduction of Exfoliated Graphite Oxide. *Carbon* **2007**, *45*, 1558−1565.
(49) Ai, K. L.; Liu, Y. L.; Lu, L. H.; Cheng, X. L.; Huo, L. H. A Novel Strategy for Making Soluble Reduced Graphene Oxide Sheets Cheaply by Adopting An Endogenous Reducing Agent. *J. Mater. Chem.* **2011**, *21*, 3365−3370.
(50) Seo, B.; Jung, G. Y.; Sa, Y. J.; Jeong, H. Y.; Chean, J. Y.; Lee, J. H.; Kim, H. Y.; Kim, J. C.; Shin, H. S.; Kwak, S. K.; Joo, S. H. Monolayer-Precision Synthesis of Molybdenum Sulfide Nanoparticles and Their Nanoscale Size Effects in the Hydrogen Evolution Reaction. *ACS Nano* **2015**, *9*, 3728−3739.
(51) Shin, S.; Jin, Z. Y.; Kwon, D. H.; Bose, R.; Min, Y. S. High Turnover Frequency of Hydrogen Evolution Reaction on Amorphous MoS_2 Thin Film Directly Grown by Atomic Layer Deposition. *Langmuir* **2015**, *31*, 1196−1202.
(52) Liu, Y.; Zhou, X. L.; Ding, T.; Wang, C. D.; Yang, Q. 3D Architecture Constructed via The Confined Growth of MoS_2 Nanosheets in Nanoporous Carbon Derived from Metal-organic Frameworks for Efficient Hydrogen Production. *Nanoscale* **2015**, *7*, 18004−18009.
(53) Zhou, W. J.; Hou, D. M.; Sang, Y. H.; Yao, S. H.; Zhou, J.; Li, G. Q.; Li, L. G.; Liu, H.; Chen, S. W. MoO_2 Nanobelts@nitrogen Self-doped MoS_2 Nanosheets as Effective Electrocatalysts for Hydrogen Evolution Reaction. *J. Mater. Chem. A* **2014**, *2*, 11358−11364.
(54) Bose, R.; Balasingam, S. K.; Shin, S.; Jin, Z. Y.; Kown, D. H.; Jun, Y.; Min, Y. S. Importance of Hydrophilic Pretreatment in the Hydrothermal Growth of Amorphous Molybdenum Sulfide for Hydrogen Evolution Catalysis. *Langmuir* **2015**, *31*, 5220−5227.
(55) Liu, N.; Guo, Y. L.; Yang, X. Y.; Lin, H. L.; Yang, L. C.; Shi, Z. P.; Zhong, Z. W.; Wang, S. N.; Tang, Y.; Gao, Q. S. Microwave-Assisted Reactant-Protecting Strategy toward Efficient MoS_2 Electrocatalysts in Hydrogen Evolution Reaction. *ACS Appl. Mater. Interfaces* **2015**, *7*, 23741−23749.
(56) Zhang, Y. F.; Zuo, L. Z.; Huang, Y. P.; Zhang, L. S.; Lai, F. L.; Fan, W.; Liu, T. X. In-Situ Growth of Few-Layered MoS_2 Nanosheets on Highly Porous Carbon Aerogel as Advanced Electrocatalysts for Hydrogen Evolution Reaction. *ACS Sustainable Chem. Eng.* **2015**, *3*, 3140−1348.
(57) Zhang, S. P.; Chowdari, B. V. R.; Wen, Z. Y.; Jin, J.; Yang, J. H. Constructing Highly Oriented Configuration by Few-Layer MoS_2: Toward High-Performance Lithium-Ion Batteries and Hydrogen Evolution Reactions. *ACS Nano* **2015**, *9*, 12464−12472.
(58) Lin, L.; Miao, N.; Wen, Y.; Zhang, S.; Ghosez, P.; Sun, Z.; Allwood, D. A. Sulfur-Depleted Monolayered Molybdenum Disulfide Nanocrystals for Superelectrochemical Hydrogen Evolution Reaction. *ACS Nano* **2016**, DOI: 10.1021/acsnano.6b04904.

DOI: 10.1021/acsami.6b06031
ACS Appl. Mater. Interfaces 2016, 8, 25210−25218